

# The Radio Afterglow From GRB 980519: A Test of the Jet and Circumstellar Models

D. A. Frail<sup>1</sup>, S. R. Kulkarni<sup>2</sup>, R. Sari<sup>3</sup>, G. B. Taylor<sup>1</sup>, D. S. Shepherd<sup>2</sup>, J. S. Bloom<sup>2</sup>, C. H. Young<sup>4,1</sup>, L. Nicastro<sup>5</sup>, N. Masetti<sup>6</sup>

## ABSTRACT

We present multi-frequency radio observations from the afterglow of GRB 980519 beginning 7.2 hours after the gamma-ray burst and ending 63 days later. The fast decline in the optical and X-ray light curves for this burst has been interpreted either as afterglow emission originating from a collimated outflow – a jet – or the result of a blast wave propagating into a medium whose density is shaped by the wind of an evolved massive star. These two models predict divergent behavior for the radio afterglow, and therefore, radio observations are capable, in principle, of discriminating between the two. We show that a wind model describes the subsequent evolution of the radio afterglow rather well. However, we see strong modulation of the light curve, which we interpret as diffractive scintillation. These variations prevent us from decisively rejecting the jet model.

*Subject headings:* gamma rays:bursts – radio continuum:general – cosmology:observations

---

<sup>1</sup>National Radio Astronomy Observatory, P. O. Box O, Socorro, NM 87801

<sup>2</sup>California Institute of Technology, Owens Valley Radio Observatory 105-24, Pasadena, CA 91125

<sup>3</sup>Theoretical Astrophysics, California Institute of Technology, MS 103-33, Pasadena, CA 91125.

<sup>4</sup>Mississippi State University, Dept. of Physics and Astronomy, MS 39762

<sup>5</sup>Istituto di Fisica Cosmica con Applicazioni all'Informatica, CNR, Via U. La Malfa 153, I-90146 Palermo, Italy

<sup>6</sup>Istituto Tecnologie e Studio Radiazione Extraterrestre, CNR, Via Gobetti 101, I-40129 Bologna, Italy

## 1. Introduction

Both geometry and environment can affect the evolution of gamma-ray burst (GRB) afterglows (Mészáros, Rees & Wijers 1998, Panaitescu, Meszaros & Rees 1998), giving us insight into such important issues as the total energetics, the burst event rate and the nature of GRB progenitors. The light curves and spectra from some of the earliest afterglows showed good agreement with fireball models of spherical blastwaves expanding into a homogeneous medium (e.g. Wijers, Rees & Mészáros 1997, Waxman 1997a). However, over the past year, we have come to recognize a class of GRBs whose afterglows exhibited steeper than normal power-law decays (i.e.  $f_\nu \propto t^{-2}$ ). Explanations for this behavior include invoking a large value for the energy spectral index ( $p \sim 4$ ) of the radiation electrons (Groot *et al.* 1998), a jet-like geometry for the relativistic shock (Rhoads 1997, Rhoads 1999, Sari, Piran & Halpern 1999), and a class of inhomogeneous circumburst medium models, specifically those shaped by the winds (mass loss) of progenitor stars (Vietri 1997, Chevalier & Li 1999, Li & Chevalier 1999).

Empirical evidence connecting GRBs to the collapse of massive stars is accumulating from studies of GRB 980425 (Galama *et al.* 1998, Kulkarni *et al.* 1998), GRB 980326 (Bloom *et al.* 1999b) and GRB 970228 (Reichart 1999, Galama *et al.* 1999). Further evidence comes from the studies of GRB environments, and includes the small measured GRB/host galaxy offsets (Bloom *et al.* 1999a, Bloom, Sigurdsson & Pols 1999) and the growing number of optically obscured afterglows such as GRB 980329 (Taylor *et al.* 1998) and GRB 970828 (Djorgovski *et al.* 1999).

The two models – the jet and the wind-shaped circumburst medium (WCM) – are well motivated by sound physical and empirical considerations. Jets have been invoked in part due to their universality, but also specifically to account for the large inferred isotropic energy release in some GRBs (e.g. GRB 990123; Kulkarni *et al.* 1999). The broad-band steepening of the optical and radio light curves seen in GRB 990510 is explained very well by the jet model (Stanek *et al.* 1999, Harrison *et al.* 1999). Likewise, if GRBs are the end points of massive stars then it is inevitable that the circumburst medium will be inhomogeneous and reflect the mass loss history of the progenitor star.

GRB 980519 occupies a central position in the debate of jets versus WCM models. It is the second brightest GRB in the BeppoSAX sample, and its X-ray and optical afterglow showed rapid fading,  $f \propto t^{-2}$  (see Halpern *et al.* 1999). Based on the optical and X-ray data Sari, Piran & Halpern (1999) advocated a jet model whereas Chevalier and Li (1999) advocate a WCM model. We discuss here the radio data in view of these two very different models.

## 2. Observations

GRB 980519 was detected on 1998 May 19.51 UT with the Wide Field Camera (WFC) on board the BeppoSAX satellite (Muller *et al.* 1998). A follow up observation with the Narrow Field Instruments (NFI) some 10 hrs after the burst detected a rapidly fading X-ray source (Nicastro *et al.* 1998) with a power-law decay slope of  $-1.83 \pm 0.3$  (Nicastro *et al.* 1999). Within the WFC error circle, and coincident with the subsequent NFI location, Jaunsen *et al.* (1998) noted a fading optical counterpart. Djorgovski *et al.* (1998) showed that the optical transient (OT) exhibited a power-law decline with  $\alpha \sim -2$ ; here  $f(t) \propto t^\alpha$ . A summary of the X-ray and optical afterglow light curves can be found in Nicastro *et al.* (1999) and Halpern *et al.* (1999), respectively.

We began observations of GRB 980519 with the Very Large Array (VLA) some 7.2 hours after the initial  $\gamma$ -ray burst. The source was clearly detected on May 22; hereafter, we will refer to the radio afterglow as VLA J232221.5+771543. A log of the VLA observations and a summary of the results can be found in Table 1. Except on the first day, when the bandwidth was halved in order to image the full WFC error circle, a 100 MHz bandwidth was used and all four Stokes parameters were measured. As these observations were begun when the VLA was in its most extended configuration and during the stormy summer season, considerable care was taken to accurately track the atmospheric phase variations across the array. Each scan on the source lasted three to five minutes and was bracketed on either side with a nearby phase calibrator (J0017+815). As a check on the integrity of the phase solutions a second phase calibrator (J2344+824) was observed frequently. The flux scale was tied to one of the sources J0137+331, J0542+498, or J1331+305.

In addition to the VLA observations, we observed the OT with the Owens Valley Radio Observatory (OVRO) six-element array on the evening of 1998 May 21. GRB 980519 was observed for 6.5 hr at a central frequency of 100 GHz with a 2 GHz bandwidth. The synthesized beam was  $5'' \times 4''$ ; see Shepherd *et al.* (1998) for the procedure used to analyze the data. The resulting map had an rms noise level of  $0.9 \text{ mJy beam}^{-1}$  and the flux at the position of the OT was  $-1.2 \text{ mJy beam}^{-1}$ . Thus we place an upper limit (mean plus  $3\sigma$ ) of  $1.5 \text{ mJy beam}^{-1}$ .

The light curve of VLA J232221.5+771543 can be found in Figure 1. The best fit position of VLA J232221.5+771543, determined by a Gaussian fit of the combined 8.46 GHz data from May 22, May 24, June 2 and June 5 is (epoch J2000)  $\alpha = 23^h 22^m 21.50^s (\pm 0.02^s)$ ,  $\delta = +77^\circ 15' 43.25'' (\pm 0.06'')$ . The radio source coincides with the OT within the errors of the optical astrometry (Jaunsen *et al.* 1998).

### 3. The Light Curve: Interstellar Scattering and Scintillation

The light curve of VLA J232221.5+771543, with a gradual rise to a plateau followed by a decline below detectability around day 60, is qualitatively similar to that of many previously studied afterglows. Even though the data are sparse it is clear that there are some large amplitude variations (e.g. around about June 7), especially at 4.86 GHz. One could attribute the variations to residual uncorrected phases caused by poor weather. Fortunately, there exists a field source J232137.6+7715.0, some 2.5' from GRB 980519. As can be seen from the two lower panels in Fig. 1, the flux of this source is stable and does not show any suppression on those days when the afterglow was not detected. Phase incoherence is a multiplicative error and the stability of J232137.6+7715.0 is an empirical confirmation of the robustness of our calibration procedure. Parenthetically we note that the field source is beyond the delay beam and is thus expected to suffer more photometric errors than a source close to the phase center.

We believe that the large variations seen in the light curve of VLA J232221.5+771543 are real, and following Goodman (1997) and Frail et al. (1997) we attribute these variations to interstellar scattering and scintillation (ISS). In particular, diffractive scintillation can induce extreme intensity variations (see below) and thereby account for the nulls in the light curve (Fig. 1). For example, in the relatively short time window of 12 to 19 days, we have four measurements with a mean of 103  $\mu$ Jy and standard deviation of 103  $\mu$ Jy at 8.46 GHz, i.e. 100% modulations. At 4.86 GHz we have mean of 80  $\mu$ Jy and standard deviation of 142  $\mu$ Jy, i.e. 180% modulations. The statistical fluctuations from thermal noise can explain about 30% and 40% of the flux modulations at 8.46 GHz and 4.86 GHz, respectively. For comparison, the field source had mean of 570  $\mu$ Jy and standard deviation of 52  $\mu$ Jy, while the statistical fluctuations are 85  $\mu$ Jy. Therefore, the modulations in our data are likely dominated by scintillation rather than by statistical noise. We now proceed with the ISS hypothesis and use the observed variability to infer the angular size of the source.

The strength of the scattering is reflected in the parameter SM, the so-called scattering measure. In the direction towards the GRB  $(l, b) = (117.96^\circ, 15.26^\circ)$ , using the formulation of Taylor & Cordes (1993) we estimate  $SM = 5.8 \times 10^{-4} \text{ m}^{-20/3} \text{ kpc}$ ; for reference, we note that this is a factor of two larger than towards GRB 970508 (Frail *et al.* 1997). We have assumed that the typical pathlength to the scattering medium in this direction is  $d_{\text{scr}}=1.9 \text{ kpc}$ . Using this SM and Goodman's equations we expect to see strong scattering for frequencies below  $\nu_0 = 15 \text{ GHz}$ . The corresponding Fresnel angle and Fresnel size at  $\nu_0$  are,  $\theta_{F_0} = 1.5 \mu\text{arcsec}$  and  $R_{F_0} = 4.2 \times 10^{10} \text{ cm}$ .

For  $\nu > \nu_0$ , the scattering is weak and the modulations scale as  $(\nu/\nu_0)^{-17/12} < 1$ . The fact that we observe order of unity fluctuations at both 4.86 GHz and 8.46 GHz implies that

$\nu_0 \geq 8.5$  GHz, compatible with the estimate from the SM. For  $\nu < \nu_0$  we will see strong diffractive scintillation only if the size of the source,  $\theta_S < \theta_D = \theta_{F_0}(\nu/\nu_0)^{6/5}$ . The other ISS parameters of interest are the decorrelation timescale (time for significant changes in the detected flux),  $t_{\text{RISS}} = 3.9 \text{ hr}(\nu/\nu_0)^{6/5}(R_{F_0}/4.2 \times 10^{10} \text{ cm})/(v_{\perp}/30 \text{ km s}^{-1})$  and the bandwidth over which the diffractive ISS is decorrelated,  $\Delta\nu = \nu_0(\nu/\nu_0)^{22/5}$ . For  $\nu_0 \simeq 15$  GHz the resulting  $(\theta_D, t_{\text{diff}}, \Delta\nu)$  are  $(0.7 \mu\text{arcsec}, 1.8 \text{ hr}, 900 \text{ MHz})$  at 8.46 GHz, and  $(0.4 \mu\text{arcsec}, 0.9 \text{ hr}, 80 \text{ MHz})$  at 4.86 GHz. In calculating  $t_{\text{RISS}}$  we have assumed a transverse speed of  $30 \text{ km s}^{-1}$  for the scintillation pattern across the line-of-sight. These estimates are rough in the sense that the estimate of SM (and hence  $\nu_0$ ), for a given pathlength, can typically fluctuate by a factor of a few. Decreasing  $\nu_0$  has the effect of increasing  $\theta_D$ ,  $t_{\text{diff}}$  and  $\Delta\nu$ .

These strong diffractive fluctuations can be suppressed under two circumstances: (1) When the duration ( $\Delta t$ ) and/or the bandwidth ( $B$ ) of the observations exceed  $t_{\text{RISS}}$  and  $\Delta\nu$ , respectively. The relevant figures of merit are given by  $n_1 = \sqrt{B/\Delta\nu}$  and  $n_2 = \sqrt{\Delta t/t_{\text{RISS}}}$ . (2) If the source size,  $\theta_S$ , exceeds  $\theta_D$ . The figure of merit here is  $n_3 = \theta_S/\theta_D$ . If either  $n_1$  or  $n_2 > 1$  then the observation will encompass more than one “scintel” (an island of constructive interference), thereby suppressing the variations. A large source will lower the modulation index to  $n_3^{-1}$  and increase the ISS timescale by the factor  $n_3$  (Narayan 1993). The fluctuations  $\delta F$  of the observed flux  $F$  in the regime of diffractive scintillation will therefore be given by

$$\frac{\delta F}{F} = \min(1, n_1^{-1}) \min(1, n_2^{-1}) \min(1, n_3^{-1}). \quad (1)$$

Our detection of strong diffractive scintillation at these frequencies suggests that all three figures  $n_1, n_2, n_3 \leq 1$ ; otherwise the fluctuations would be suppressed. From Table 1 and the estimate of the ISS parameters above we find  $n_1(4.86 \text{ GHz}) \sim 1$ ,  $n_1(8.46 \text{ GHz}) \sim 0.1$  and  $n_2(4.86 \text{ GHz}) \sim 2$ ,  $n_2(8.46 \text{ GHz}) \sim 1$ . These estimates are compatible with the constraint discussed above. Interestingly, if  $\nu_0$  were any larger than 15 GHz, the fluctuations would have been suppressed since both  $n_1$  and  $n_2$  would have become larger than unity at 4.86 GHz. Our observations, therefore, limit  $\nu_0$  to a narrow range of values (8 – 15 GHz) and likewise the estimates of  $\theta_D, t_{\text{diff}}, \Delta\nu$ .

Thus, given the uncertainties involved, the strong modulations seen at both frequencies are quite reasonable. Furthermore, the strong modulations require that  $n_3$  be close to unity i.e. the source must be less than  $\theta_D$ . Thus if our explanation that the strong variation seen in the light curve is due to diffractive ISS is correct, then the radio source must be less than  $0.4 \mu\text{arcsec}$  – a very small size indeed. Theoretical models predict a somewhat larger size. We will discuss this discrepancy in §4.

The strong modulations caused by scintillation do not allow us to accurately estimate

the spectral slope in the radio band. However, averaging over all observations from day 12 on we find  $\beta \cong -0.45 \pm 0.6$  (where  $f_\nu \propto \nu^\beta$ ). This large range is compatible with both the early spectral index of  $1/3$  expected at low frequencies and with the late spectral index of  $\sim -1$ . It is inconsistent with the self-absorption spectral index of 2. The source was never detected at 1.43 GHz (see Table 1). We conclude that VLA J232221.5+771543 is an extremely compact ( $< 1 \mu\text{arcsec}$ ) source with a self absorption frequency  $\nu_{ab}$  between 1.43 GHz and 4.86 GHz.

#### 4. Discussion

The intense interest in GRB 980519 primarily stems from the fact that it was one of the first GRBs to be recognized to have a rapidly fading afterglow (Halpern *et al.* 1999). Two entirely different models were proposed to account for the rapid fading: a jet expanding into a homogeneous medium (Sari, Piran & Halpern 1999) and a spherical explosion into a wind-shaped circumburst medium (WCM; Chevalier & Li 1999). Both Sari *et al.* and Chevalier & Li used the same optical and X-ray data but ended up favoring two radically different models.

The currently accepted view is that the afterglow emission arises in the forward shock of relativistically moving material ejected from a compact source (e.g. Mészáros & Rees 1997, Waxman 1997b). It is assumed that in this shock the electrons are accelerated to a power-law distribution of energies (index  $p$ ) above some minimum energy,  $\gamma_m m_e c^2$ . Furthermore, it is assumed that there is a suitably strong magnetic field in the post-shock region. The energy density of the electrons and the magnetic field is assumed to scale linearly with the energy density of the protons. Gyration of the electrons in the magnetic field then results in a broad-band spectrum characterized by three frequencies,  $\nu_{ab}$ ,  $\nu_m$  and  $\nu_c$  and the flux at frequency  $\nu_m$ ,  $f_m$  (Sari, Piran & Narayan 1998). The slope above  $\nu_m$  is given by  $f_\nu \propto \nu^{-(p-1)/2}$ , and this steepens by one half at  $\nu_c$  due to radiative cooling. Below  $\nu_m$  the spectral slope is the classical  $f_\nu \propto \nu^{1/3}$ , until it turns over below  $\nu_{ab}$  due to synchrotron self-absorption, for which  $f_\nu \propto \nu^2$ . The dynamics of the expansion, the density distribution of the circumstellar matter and the details of the energy injection govern the the temporal evolution of these four parameters. However, the basic shape of the above spectrum does not change. Thus the key to distinguishing between competing models is through following the temporal evolution of the spectrum.

Characterizing the broad-band spectrum by  $f(\nu, t) \propto t^\alpha \nu^\beta$ , we note from Halpern *et al.* (1999) in the first 1 – 2 days after the burst the following:  $\alpha_{\text{opt}} = -2.05 \pm 0.04$ ,  $\beta_{\text{opt}} = -1.20 \pm 0.25$ ,  $\alpha_X = -1.83 \pm 0.30$  and  $\beta_{\text{opt-X}} = -1.05 \pm 0.10$ . Within errors the X-ray

afterglow declines as rapidly as the better measured optical afterglow. Likewise, within errors, the optical spectral index,  $\beta_{\text{opt}}$  is the same as the better measured optical-X-ray spectral index,  $\beta_{\text{opt-X}}$ . Hereafter we will refer to  $\alpha_{\text{opt}}$  and  $\beta_{\text{opt-X}}$  by  $\alpha$  and  $\beta$ .

Each model has a specific closure relation between  $\alpha$  and  $\beta$ . We now consider each model in turn. (1) A spherical explosion in a constant density medium would require  $H = 0$  or  $H = 1/2$  depending on whether the range of observing frequencies is below or above  $\nu_c$ ; here  $S(\alpha, \beta) \equiv \alpha - 3/2\beta$ . The measured  $H = -0.48 \pm 0.16$  rules out this model (Halpern et al. 1999, Sari, Piran, & Halpern 1999). (2) A jet model would need  $J(\alpha, \beta) \equiv \alpha - 2\beta = -1, 0$  depending on whether the range of observing frequencies is below or above  $\nu_c$ . We find  $J = 0.05 \pm 0.21$  which is seemingly more consistent with a jet expanding into a constant density medium with both the optical and X-ray frequencies below  $\nu_c$ . Sari et al. (1999) and Halpern et al. (1999) favor a jet model but with  $\nu_c$  between the optical and X-ray bands, in order to explain  $\beta$  with a standard value of  $p \sim 2.4$ . The apparent inconsistency with the value of  $J$  is attributed, in this interpretation, to the theoretically very long transition (Panaitescu, Meszaros & Rees 1998, Rhoads 1999, Sari, Piran & Halpern 1999) to the jet asymptotic power-law. The observed value of  $\alpha$  may therefore be less than the theoretical one, if measured on a finite time interval. (3) An impulsive explosion in wind-shaped circumstellar model would need  $W(\alpha, \beta) = 2\alpha - 3\beta = -1, 1$  depending on whether the range of observing frequencies is below or above  $\nu_c$ . We find  $W = -0.95 \pm 0.3$  which is consistent with this model provided that both the optical and X-ray frequencies are below  $\nu_c$ . Chevalier & Li (1999) justify the WCM model on this basis. However, they do note that their estimated  $\nu_c$  on day 1 (when  $\alpha$  and  $\beta$  were measured) is between the optical and X-ray bands and argue that given the scanty measurements and rough theory the inconsistency is not particularly worrisome.

Thus both the jet model and the WCM model can account for the observed optical and X-ray afterglow observations including the rapid decay. In the WCM model, the rapid decline is due to the gas density in the wind falling off as the inverse square of the distance between the shock boundary and the burst location, together with a larger value of the electron powerlaw index  $p \sim 3$ . In the jet model, the decrease is due to geometry. Due to relativistic “beaming”, only a small portion of the shocked gas is visible to the observer, a solid angle  $\Gamma^{-2}$  where  $\Gamma$  is the bulk Lorentz factor of the shocked gas. When  $\Gamma$  falls below  $\theta_J^{-1}$ , the inverse of the opening angle of the jet, the observer will notice the finite edge of the emitting surface, thereby leading to a deficit of emission and thus a steeper than normal decline. Moreover, at about the same time, the jet will begin to expand sidewise, further enhancing the decline.

We now discuss how radio observations can help resolve the ambiguity of the choice of

models. For the sake of completeness, we also include a discussion of the simplest afterglow model (spherical explosion in a homogeneous medium).

**Spherical, homogeneous model.** In this model,  $\nu_{ab} \propto t^0$ ,  $\nu_m \propto t^{-3/2}$  and  $f_m = t^0$ . As discussed in §3,  $\nu_{ab} < 8.46 \text{ GHz} < \nu_m$ ; this is certainly a secure statement two days after the burst. In this frequency range, we expect  $f(t) \propto t^{1/2}$  until  $\nu_m$  reaches 8.46 GHz; we estimate (in the framework of this model) this will happen around 140 d. This estimate relies on a knowledge of the basic spectral shape of the afterglow (Sari, Piran & Narayan 1998) and the near simultaneous optical and radio data on 1998 May 28.59 UT to derive  $\nu_m$  and  $f_m$  at this time and evolve it forward until  $\nu_m=8.46 \text{ GHz}$ . Thereafter the radio flux will decay in a manner similar to the optical and X-ray flux. As can be seen from Figure 2 the predictions are clearly inconsistent with the observations. Even the strong modulations produced by the ISS are unable to resolve this discrepancy (see below). Thus we can reject the spherical model in an entirely independent way from the closure method.

**Jet Model.** We begin by noting that the steep optical decline had already started at the time of the first afterglow observation ( $t_1$ ) – the I-band observation by Jaunsen et al. (1998) about 7.5 hr after the burst. Thus the epoch at which the jet-like geometry of the emitting surface becomes apparent to the observer,  $t_J$ , is less than  $t_1$ . The epoch of the I-band observations is close to our first radio observation (see Table 1). In this “jet-dominated” regime the radio afterglow emission is  $f(\nu_{ab} < \nu < \nu_m) \propto t^{-1/3}$  and  $f(\nu < \nu_{ab}) \propto t^0$  (Sari et al. 1999). However, in §2 we argued that VLA J232221.5+771543 is an absorbed source with  $\nu_{ab}$  between 1.43 and 4.86 GHz. The self-absorption frequency evolves slowly with time,  $\nu_{ab} \propto t^{-1/5}$ . Thus we expect 8.46 GHz to be in the optically thin regime and therefore the flux at this frequency should decrease as  $\propto t^{-1/3}$ . A  $t^{-1/3}$  fit to the data, does not give a reasonable  $\chi^2$ . However, the errors in the flux density (as quoted in Table 1) may be underestimating the real uncertainties for a strongly scintillating source. If we fit the data, allowing for strong diffractive scintillation in the measurement uncertainties (i.e.  $\sigma = \bar{S}$ ) then a reasonable solution can be found  $S=210 t_d^{-1/3} \mu\text{Jy}$  ( $\chi^2=6$  with 13 dof), where  $t_d$  is time in days. The sharp break in the light curve at  $t_m = 26$  days corresponds to  $\nu_m=8.46 \text{ GHz}$  and was derived by evolving the spectrum forward from  $t = 1.08$  days (with  $\beta=1/3$  for  $\nu < \nu_m$  and  $\beta = \beta_{\text{opt-X}}$  for  $\nu > \nu_m$ ), when high quality optical and radio data existed.

**Wind-shaped Circumstellar Medium Model.** Using the contemporaneous X-ray, optical and radio data taken up to three days after the burst, Chevalier & Li (1999) fit the circumstellar model to derive the fireball parameters (total energy, energy power law index, fraction of energy in electrons and magnetic fields) and the wind properties, for an assumed redshift of  $z=1$ . In their derivation, the 8.46 GHz emission initially originates below  $\nu_{ab}$  and  $\nu_m$  but the subsequent evolution moves them into this band as  $\nu_{ab} \propto t^{-3/5}$ ,  $\nu_m \propto t^{-3/2}$  and



$f_m \propto t^{-1/2}$ . Thus in the circumstellar model one predicts an initial rise of the radio flux as the source opacity decreases, followed by a plateau when  $\nu_{ab} < 8.46 \text{ GHz} < \nu_m$  and then a steep decay when  $\nu_m < 8.46 \text{ GHz}$ . We have plotted the model fit of Chevalier & Li (1999) (labeled “Wind”) in Fig. 2. We stress that the model was derived on the first three days of afterglow data, spanning 8 orders of magnitude in frequency, and yet without any further adjustments their model fits the next 60 days of VLA measurements remarkably well.

As we have noted in the previous section, the angular size of the afterglow is less than  $1 \mu\text{arcsec}$  even after about 15 days. In the three models, spherical, wind and jet, the afterglow angular size at that time is given by

$$\theta_{\text{Sphere}} = 2.8 \mu\text{arcsec} \left( \frac{1+z}{2} \right)^{-5/8} D_{A,28}^{-1} E_{52}^{1/8} n_i^{-1/8} (t/15 \text{ days})^{5/8} \quad (2)$$

$$\theta_{\text{Wind}} = 2.2 \mu\text{arcsec} \left( \frac{1+z}{2} \right)^{-3/4} D_{A,28}^{-1} E_{52}^{1/4} A_{\star}^{-1/4} (t/15 \text{ days})^{3/4} \quad (3)$$

$$\theta_J = 1.7 \mu\text{arcsec} \left( \frac{1+z}{2} \right)^{-5/8} D_{A,28}^{-1} E_{52}^{1/8} n_i^{-1/8} (t_J/8 \text{ hr})^{1/8} (t/15 \text{ days})^{1/2}. \quad (4)$$

Here,  $D_{A,28}$  is the distance in units of  $10^{28} \text{ cm}$ ,  $E_{52}$  is the inferred “isotropic” energy released in the explosion in units of  $10^{52} \text{ ergs}$ ,  $n_i$  is the surrounding density in the constant density case.  $A_{\star}$  characterizes the wind density as  $\rho(R) = 5 \times 10^{11} A_{\star} R_{\text{cm}}^{-2} \text{ g cm}^{-3}$ , with as a  $R_{\text{cm}}$  the wind radius in cm. These sizes are quite similar to each other. This stems from the very low dependence of the size as a function of density and from the fact that the density in front of the shock, at a time of 15 days, in a wind model with typical parameters is not very different from regular ISM densities. It can be seen that the small inferred size from the scintillation is challenging for all these models. It requires either a dense wind, or a jet with very small opening angle, that begins to spread at a very early time. It is hard to reduce the size below  $1 \mu\text{arcsec}$  for any reasonable choice of the parameters in the spherical constant density model. The agreement with scintillation theory would improve if either SM or the effective distance of the scattering screen  $d_{\text{scr}}$  were lower by a factor of two. Along specific lines of sight the uncertainty in either of these quantities could vary by this amount due to the non-uniform nature of the ionized medium. In such a case the inferred size of  $0.4 \mu\text{arcsec}$  would increase by a factor of 2.5, enabling both jet and wind models to fit the data.

## 5. Conclusions

The observed steep decline in the optical and X-ray light curves of the afterglow from GRB 980519 lends itself to two equally compelling hypotheses, the first being that the

afterglow emission originates from a collimated outflow (or jet), and the second, that the emission is the result of a blast wave propagating into a medium whose density is shaped by the wind of an evolved massive star. These competing models predict divergent behavior for the evolution of the radio emission. In the jet model the radio flux is expected to decrease continuously after the jet edge becomes visible. In contrast, the circumstellar model, specifically the Wolf-Rayet wind model of Chevalier & Li (1999), predicts a linear rise, followed by a broad plateau and a late decay in the radio light curve.

In this case, scintillation, low-signal-to-noise and sparse data at early times, has limited us from decisively choosing either model. The influence of ISS could be reduced, in future afterglow observations, if one has more measurements at early times (the first two days is where the models differ the most). Such observations, separated by a few hours (a time which is larger than  $t_{ISS}$ ), could be averaged to produce a more solid estimate of the emitted flux, free of large modulations. Nevertheless, this result illustrates the unique diagnostics provided by radio observations and its potential for unraveling the origin of GRBs. Previous examples include the demonstration of jets in GRB 990510 (Harrison *et al.* 1999) and the discovery of a reverse shock in GRB 990123 (Sari & Piran 1999, Kulkarni *et al.* 1999).

DAF thanks Roger Chevalier and Zhi-Yun Li for providing their model light curves. SRK thanks Jim Cordes for discussions related to ISS. The Very Large Array (VLA) is operated by the National Radio Astronomy Observatory, a facility of the National Science Foundation operated under cooperative agreement by Associated Universities, Inc. SRK's research is supported by grants from NSF and NASA. RS is supported by the Sherman Fairchild Foundation.

## REFERENCES

- Bloom, J. S. *et al.* 1999a, ApJ, 518, L1.
- Bloom, J. S. *et al.* 1999b, Nature, 401, 453.
- Bloom, J. S., Sigurdsson, S., and Pols, O. R. 1999, MNRAS, 305, 763.
- Chevalier, R. A. and Li, Z.-Y. 1999, ApJ, 520, L29.
- Djorgovski, S. G., *et al.* 1999, in preparation.
- Djorgovski, S. G., Gal, R. R., Kulkarni, S. R., Bloom, J. S., and Kelly, A. 1998, GCN notice 79.
- Frail, D. A., Kulkarni, S. R., Nicastro, S. R., Feroci, M., and Taylor, G. B. 1997, Nature, 389, 261.
- Galama, T. J. *et al.* 1998, Nature, 395, 670.
- Galama, T. J. *et al.* 1999, ApJ. submitted, astro-ph/9907264.
- Goodman, J. 1997, New Astr., 2(5), 449.
- Groot, P. J. *et al.* 1998, ApJ, 502, L123.
- Halpern, J. P., Kemp, J., Piran, T., and Bershadsky, M. A. 1999, ApJ, 517, L105.
- Harrison, F. A. *et al.* 1999, ApJ, 523, L121.
- Jaunsen, A. O., Hjorth, J., Andersen, M. I., Kjærsmo, K., Pedersen, H., and Palazzi, E. 1998, GCN notice 78.
- Kulkarni, S. R. *et al.* 1999, ApJ, 522, L97.
- Kulkarni, S. R. *et al.* 1998, Nature, 395, 663.
- Li, Z.-Y. and Chevalier, R. A. 1999, In Press, ApJ, astro-ph/9903483.
- Mészáros, P. and Rees, M. J. 1997, ApJ, 476, 232.
- Mészáros, P., Rees, M. J., and Wijers, R. A. M. J. 1998, ApJ, 499, 301.
- Muller, J. M., Heise, J., Butler, C., Frontera, F., Di Ciolo, L., Gandolfi, G., Coletta, A., and Soffitta, P. 1998, IAU Circ., 6910.

- Narayan, R. 1993, in Pulsars as Physics Laboratories, ed. A. G. Lyne R. D. Blandford, A. Hewish and L. Mestel, Oxford University Press, 151.
- Nicastro, L. *et al.* 1999, in press A&AS , astro-ph/9904169.
- Nicastro, L., Antonelli, L. A., Celidonio, G., Daniele, M. R., De Libero, C., Spoliti, G., Piro, L., and Pian, E. 1998, IAU Circ., 6912.
- Panaiteescu, A., Meszaros, P., and Rees, M. J. 1998, ApJ, 503, 314.
- Reichart, D. E. 1999, ApJ, 521, L111.
- Rhoads, J. E. 1997, ApJ, 487, L1.
- Rhoads, J. E. 1999, Submitted to ApJ; astro-ph/9903399.
- Sari, R. and Piran, T. 1999, ApJ, 517, L109.
- Sari, R., Piran, T., and Halpern, J. P. 1999, ApJ, 519, L17.
- Sari, R., Piran, T., and Narayan, R. 1998, ApJ, 497, L17.
- Shepherd, D. S., Frail, D. A., Kulkarni, S. R., and Metzger, M. R. 1998, ApJ, 497, 859.
- Stanek, K. Z., Garnavich, P. M., Kaluzny, J., Pych, W., and Thompson, I. 1999, ApJ, 522, L39.
- Taylor, G. B. *et al.* 1998, ApJ, 502, L115.
- Taylor, J. H. and Cordes, J. M. 1993, ApJ, 411, 674.
- Vietri, M. 1997, ApJ, 488, 105.
- Waxman, E. 1997a, ApJ, 491, L19.
- Waxman, E. 1997b, ApJ, 489, L33.
- Wijers, R. A. M. J., Rees, M. J., and Mészáros, P. 1997, MNRAS, 288, L51.

Table 1. VLA Observations of GRB 980519

Epoch (UT)	$\Delta t$ (days)	TOS (min)	$S_{8.46} \pm \sigma$ ( $\mu\text{Jy}$ )	$S_{4.86} \pm \sigma$ ( $\mu\text{Jy}$ )	$S_{field} \pm \sigma$ ( $\mu\text{Jy}$ )	$S_{1.43} \pm \sigma$ ( $\mu\text{Jy}$ )
1998 May 19.81	0.30	99	49 $\pm$ 28			
1998 May 20.59	1.08	54	64 $\pm$ 27			
1998 May 22.35	2.84	112	103 $\pm$ 19			
1998 May 24.96	5.45	112	127 $\pm$ 20			
1998 May 31.54	12.03	132	40 $\pm$ 25	25 $\pm$ 27	591 $\pm$ 80	
1998 Jun. 02.56	14.05	125	142 $\pm$ 29	292 $\pm$ 41	607 $\pm$ 100	
1998 Jun. 05.14	16.63	106	230 $\pm$ 31	16 $\pm$ 33	596 $\pm$ 80	
1998 Jun. 07.43	18.92	183	1.2 $\pm$ 32	–13 $\pm$ 37	493 $\pm$ 82	–4.5 $\pm$ 34
1998 Jun. 11.94	23.43	69	82 $\pm$ 40	215 $\pm$ 44	537 $\pm$ 90	
1998 Jun. 18.58	30.07	78	66 $\pm$ 23	5 $\pm$ 31	676 $\pm$ 70	
1998 Jul. 07.26	48.75	100	78 $\pm$ 27	133 $\pm$ 42	480 $\pm$ 71	
1998 Jul. 20.23	61.72	124	0.9 $\pm$ 30	190 $\pm$ 40	356 $\pm$ 73	15 $\pm$ 42
1998 Jul. 21.25	62.74	94	42 $\pm$ 32	57 $\pm$ 45	480 $\pm$ 79	–35 $\pm$ 58

Note. — The columns are (left to right), (1) UT date of the start of each observation, (2) time elapsed since the GRB 980519 event, (3) total duration of the observing run, (4) 8.46 GHz flux density of the radio transient (RT), with the error given as the root mean square flux density, (5) 4.86 GHz flux density of the RT, (6) The integrated 4.86 GHz flux density of J232137.6+7715.0, a field source 2.5' from the GRB, and (7) 1.43 GHz flux density of the RT.

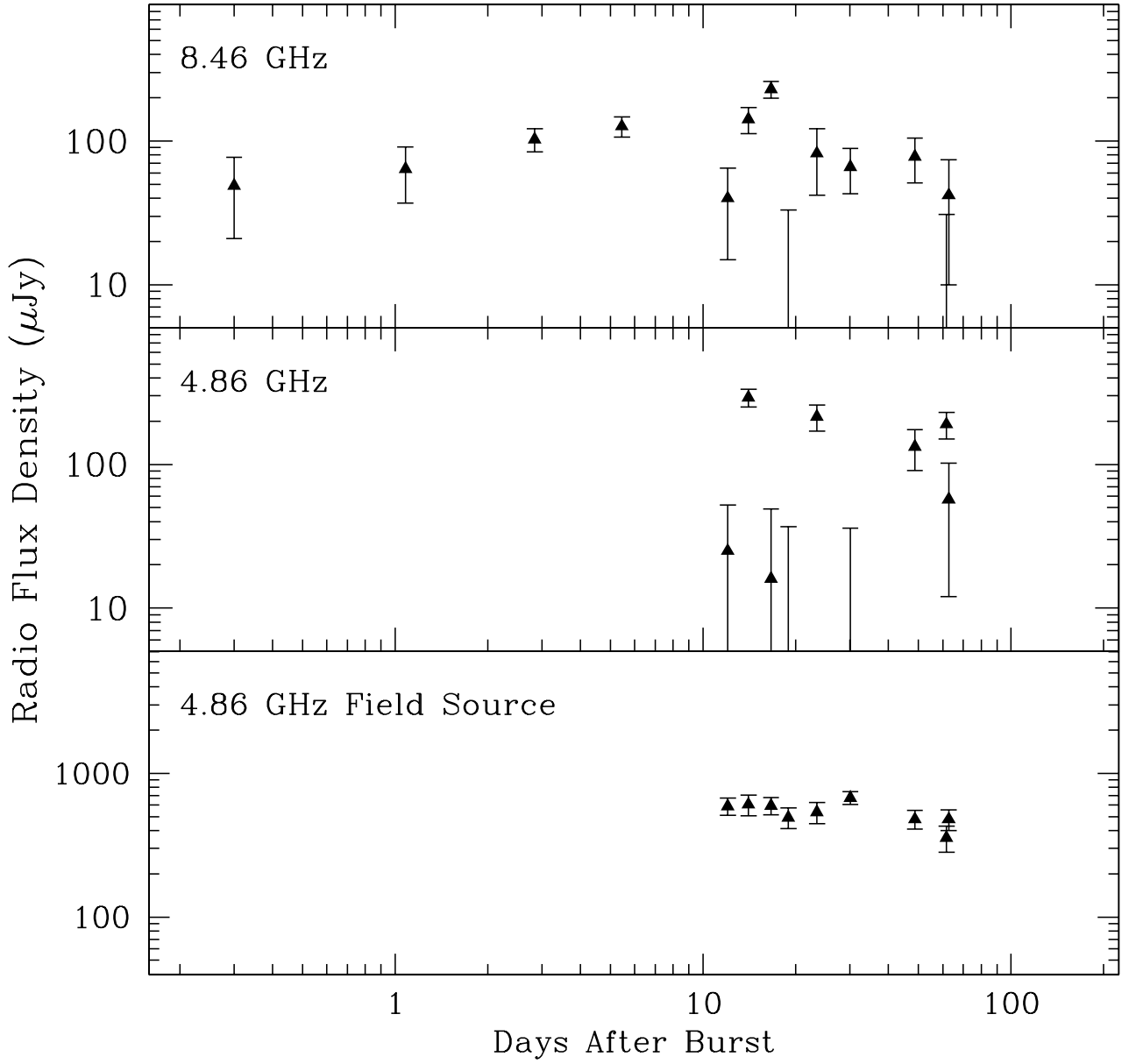


Fig. 1.— Observed radio lightcurves at 8.46 GHz and 4.86 GHz. The two top panels are light curves for the radio afterglow from GRB 980519, while the bottom panel is the light curve for J232137.6+7715.0, a field source 2.5' from the GRB. Flux densities (and errors) are taken from Table 1.

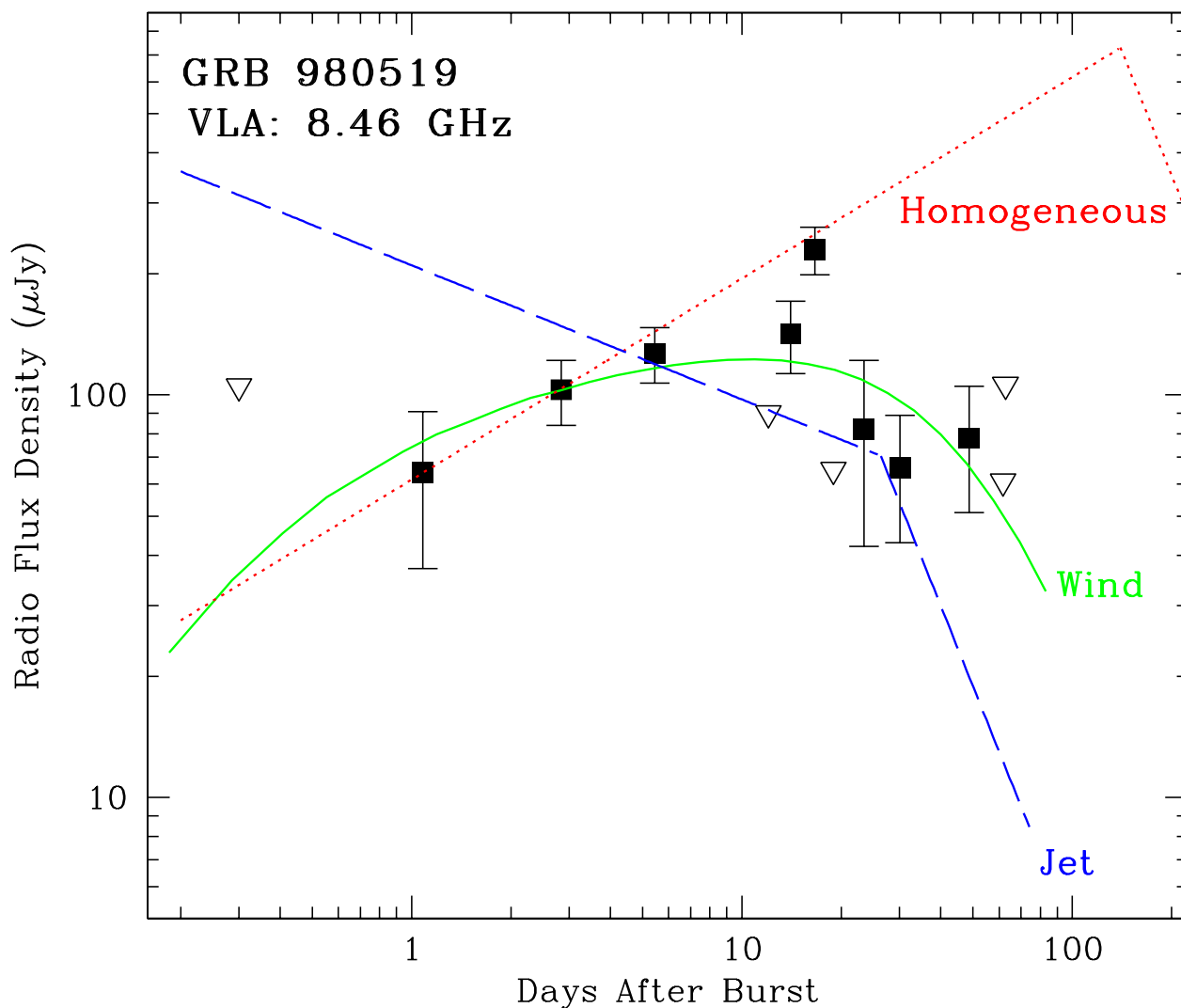


Fig. 2.— Observed and model lightcurves at 8.46 GHz. Detections are indicated by the filled squares. Upper limits for the non-detections (open triangles), are plotted as the measured flux at the position of the radio transient plus twice the rms noise. Three different model predictions are plotted. The circumstellar model “Wind” is taken directly from Chevalier & Li (1999) with no modifications. The basic adiabatic, forward shock model with spherical expansion into a homogeneous medium is indicated as “Homogeneous”. The predicted behavior for the jet model of Sari et al. (1999) is given by “Jet”. See text for additional details.